The Journal of Experimental Medicine

Intratumoral IL-12 combined with CTLA-4 blockade elicits T cell–mediated glioma rejection

Johannes vom Berg,[1] Melissa Vrohlings,[1] Sergio Haller,[1] Aladin Haimovici,[1] Paulina Kulig,[1] Anna Sledzinska,[1] Michael Weller,[2] and Burkhard Becher[1]

[1]Institute of Experimental Immunology, University of Zurich, 8057 Zurich, Switzerland
[2]Department of Neurology, University Hospital Zurich, 8091 Zurich, Switzerland

Glioblastomas (GBs) are the most aggressive form of primary brain cancer and virtually incurable. Accumulation of regulatory T (T reg) cells in GBs is thought to contribute to the dampening of antitumor immunity. Using a syngeneic mouse model for GB, we tested whether local delivery of cytokines could render the immunosuppressive GB microenvironment conducive to an antitumor immune response. IL-12 but not IL-23 reversed GB-induced immunosuppression and led to tumor clearance. In contrast to models of skin or lung cancer, IL-12–mediated glioma rejection was T cell dependent and elicited potent immunological memory. To translate these findings into a clinically relevant setting, we allowed for GB progression before initiating therapy. Combined intratumoral IL-12 application with systemic blockade of the co-inhibitory receptor CTLA-4 on T cells led to tumor eradication even at advanced disease stages where monotherapy with either IL-12 or CTLA-4 blockade failed. The combination of IL-12 and CTLA-4 blockade acts predominantly on CD4+ cells, causing a drastic decrease in FoxP3+ T reg cells and an increase in effector T (T eff) cells. Our data provide compelling preclinical findings warranting swift translation into clinical trials in GB and represent a promising approach to increase response rates of CTLA-4 blockade in solid tumors.

CORRESPONDENCE
Burkhard Becher:
becher@immunology.uzh.ch

Abbreviations used: ADCC, antibody-dependent cell-mediated cytotoxicity; BLI, bioluminescence imaging; CTLA-4, cytotoxic T-lymphocyte-associated antigen 4; GB, glioblastoma; HPRT, hypoxanthine-guanine phosphoribosyltransferase; ILC, innate lymphoid cells; i.t., intratumoral; MFI, mean fluorescent intensity; NKT, NK T cells; *Prf1*, *Perforin*; ROI, region of interest; T eff, effector T; TIL, tumor-infiltrating lymphocyte; T reg, regulatory T.

Glioblastoma (GB) is among the most aggressive cancers known. Current treatment options are limited and the clinical prognosis is poor. Patients diagnosed with GB show a median survival of little more than a year despite aggressive surgery, radiation therapy, and chemotherapy (Weller et al., 2013). Moreover, GBs induce a highly immunosuppressive microenvironment, characterized by the presence of T reg cells (Grauer et al., 2007; Jacobs et al., 2010). Given the failure of conventional therapy in GBs, the most promising treatment option may thus rely on the exploration of immunotherapeutic strategies. IL-12 is the prototype member of a group of heterodimeric cytokines with predominantly proinflammatory properties. IL-12 polarizes naive helper T cells (T_H) to adopt a T_H1 phenotype and

stimulates cytotoxic T cells, NK T (NKT) cells, and conventional NK cells. The therapeutic success of application of IL-12 in various preclinical animal models of cancer is compelling (Colombo and Trinchieri, 2002). However, in humans, systemic delivery of IL-12 evoked serious adverse events such as leukopenia and thrombocytopenia, including fatalities in two patients, at moderately effective doses (Atkins et al., 1997; Leonard et al., 1997). Thus, local rather than systemic delivery of IL-12 represents the only viable option for using IL-12 in cancer immunotherapy in humans. IL-12 appears to exert its cancer-suppressive properties through different effector cells in a tissue-specific manner. In the B16 melanoma model, IL-12–mediated suppression of s.c. tumor growth is mediated by a small

population of IL-12–responsive, Rorγt-dependent innate lymphoid cells (ILCs; Eisenring et al., 2010). On the other hand, B16-derived lung tumors are controlled through IL-12–activated NK cells (Kodama et al., 1999; Eisenring et al., 2010). Conversely, IL-12–mediated glioma control has been attributed to T cells and NK cells, but open questions remain about which cell types indeed are the precise cellular targets of IL-12, consequently mediating anti-GB immunity (Vetter et al., 2009; Yamanaka et al., 2002, 2003). IL-23 is another member of the IL-12 family and also has potent pro-inflammatory properties. Several groups reported potent antitumor activity in various experimental settings including brain tumors (Lo et al., 2003; Hu et al., 2006). Others have reported a protumorigenic effect of IL-23 (Langowski et al., 2006). The goal of this study was to systematically analyze whether and how IL-12 and IL-23 induce an antitumor immune response in a syngeneic murine model of GB.

RESULTS AND DISCUSSION

To determine whether IL-12 and IL-23 are suitable candidates to overcome the local immunosuppressive environment in GB and to trigger rejection, we expressed either of these two cytokines in C57BL/6 syngeneic GL-261 mouse glioma cells (Szatmári et al., 2006). First, we generated a GL-261 line that constitutively expressed *Photinus pyralis* luciferase (hereafter, termed GL-261luc) for bioluminescence imaging (BLI). We next modified this cell line to continuously release a fusion protein of IL-12 or IL-23 joined to the crystallizable fragment of mouse IgG3 (IL-12Fc or IL-23Fc) or the IgG fragment alone as control (termed GL-261luc:IL-12, GL-261luc:IL-23, and GL-261luc:Fc, respectively). Cytokine production and BLI were equivalent among transfected cells (unpublished data). Expression levels of MHCI and II and proliferation were comparable to parental cells (Fig. 1, A and B), as was the median survival of animals inoculated with GL-261luc:Fc (Fig. 1 C).

We implanted GL-261luc:IL-12 or GL-261luc:IL-23 intracranially into C57BL/6 mice and compared growth with GL-261luc:Fc, monitoring BLI and survival (Fig. 1, D and E). While IL-23 secretion appeared to be mildly tumor promoting (Fig. 1 D), IL-12 expression conferred a clear survival advantage (Fig. 1 E). This was not a tumor intrinsic effect, as GL-261luc:Il-12 displayed progressive growth in *Il12rb2*$^{-/-}$ hosts (unpublished data). On day 35 after injection, we detected only a residual tumor in some animals injected with GL-261luc:IL-12, whereas mice challenged with GL-261luc:IL-23 or GL-261luc:Fc showed robust tumor formation when analyzed histologically (Fig. 1, G). This contrasts studies on IL-23–induced glioma rejection using neural stemlike cell– or DC-based approaches that showed potent antiglioma activity (Hu et al., 2006; Yuan et al., 2006). However, in various other models of solid tumors, it is also becoming increasingly apparent that IL-23 has primarily protumorigenic effects (Ngiow et al., 2013). Therefore, for the remainder of this study, we focused on the effector mechanisms of IL-12–mediated glioma rejection.

Longitudinal analysis via histology and flow cytometry of the tumor–infiltrating lymphocyte (TIL) composition revealed

that T cells and NK cells were readily detected within tumors 2 wk after tumor implantation (unpublished data). To systematically examine the contribution of specific leukocyte populations, we challenged a series of mouse mutants with intracranial GL-261luc:IL-12. We used mice lacking T and B cells (*Rag1*$^{-/-}$), conventional NK cells (*Il15ra*$^{-/-}$), or mice lacking T, B, NK cells, as well as ILCs (*Rag2*$^{-/-}$ *Il2rg*$^{-/-}$; Fig. 2 A). Tumor protection was lost in *Rag2*$^{-/-}$ *Il2rg*$^{-/-}$ and *Rag1*$^{-/-}$ animals, whereas *Il15ra*$^{-/-}$ mice were able to control the tumor, suggesting that adaptive lymphocytes are absolutely required for IL-12–mediated glioma rejection. The fact that the loss of NK cells and ILCs in *Rag2*$^{-/-}$ *Il2rg*$^{-/-}$ mice did not change the clinical course compared with *Rag1*$^{-/-}$ mice, combined with the ability of *Il15ra*$^{-/-}$ mice to reject GL-261luc:IL-12, demonstrates that NK cells and ILCs were largely dispensable for IL-12–mediated tumor rejection. We also investigated the contribution of CD4 and CD8 T cells using MHCII (*Ia(b)*$^{-/-}$)- and MHCI (β$2m$$^{-/-}$)-deficient mice, respectively. In contrast to WT mice, *Ia(b)*$^{-/-}$ mice did not control GL-261luc:IL-12 tumors, and β$2m$$^{-/-}$ mice succumbed to the gliomas shortly thereafter (Fig. 2 B). Although there is precedence for a role of NKT cells in IL-12–mediated tumor rejection (Cui et al., 1997), the effective IL-12–mediated tumor rejection in *Il15ra*$^{-/-}$ mice further dismisses a critical role of NK and NKT cells because both populations depend on IL-15R signaling (Gordy et al., 2011).

To further characterize the T cell–dependent tumor control, we tested for immunological memory formation in the surviving mice that had been previously challenged with GL-261luc:IL-12 cells (Fig. 2 C). In contrast to the primary challenge, we now injected GL-261luc:Fc cells into the contralateral hemisphere of survivors or naive WT animals. In agreement with earlier studies (Daga et al., 2007; Liu et al., 2002), we observed a rapid rejection of the newly implanted tumors within days in rechallenged survivors. Whereas BLI at day 1 after injection suggested identical tumor cell seeding across the two groups, only the naive mice exhibited a steadily increasing signal (Fig. 2 C), suggesting memory formation.

IL-12 is recognized for its capacity to polarize IFN-γ–producing T$_H$1 cells. However, *Ifng*$^{-/-}$ mice rejected GL-261luc:IL-12 cells (Fig. 2 D) at a similar rate as WT animals, suggesting that the mechanism by which IL-12 induces tumor rejection is largely independent of IFN-γ. Conversely, IL-12 also stimulates the cytotoxic activity of T cells. We analyzed the role of perforin, a cytolytic molecule primarily expressed by CD8$^+$ CTLs and NK cells. In contrast to *Ifng*$^{-/-}$ mice, *Prf1*$^{-/-}$ mice failed to control the tumor (Fig. 2 E). This further shows that perforin-mediated T cell cytotoxicity is the major effector mechanism of IL-12–mediated glioma rejection.

Previous studies investigated the mechanisms of IL-12 in glioma rejection, many of these in a DC vaccination setting (Joki et al., 1999; Yamanaka et al., 2002, 2003). A crucial involvement of NK cells and T cells (CD4$^+$ and/or CD8$^+$) in the IL-12–mediated rejection of experimental gliomas was described (Joki et al., 1999; Yamanaka et al., 2002, 2003). These reports present contradictory findings regarding the contribution
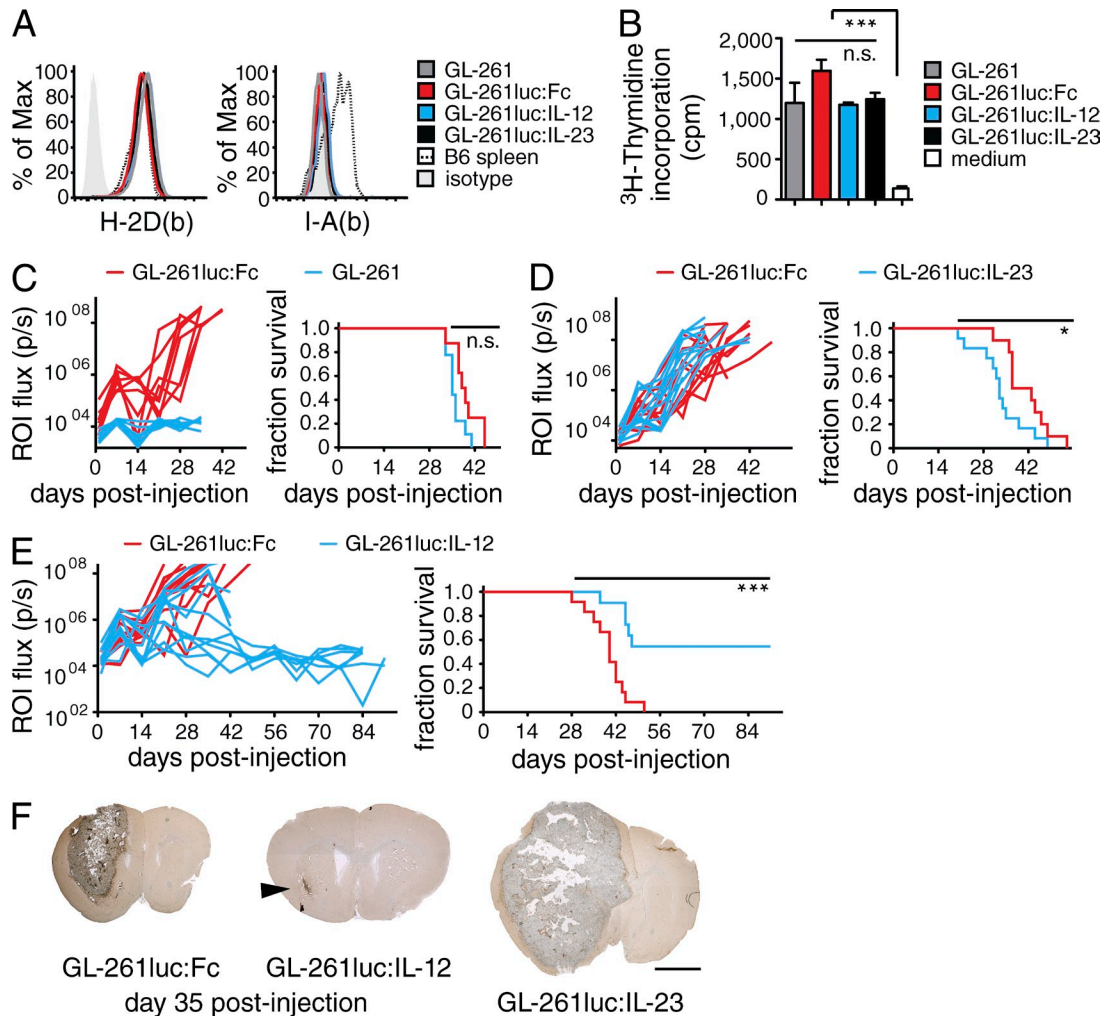
Figure 1. Intratumoral expression of IL–12 but not IL–23 leads to rejection of experimental gliomas. (A and B) In vitro analysis of GL-261, GL-261luc:Fc, GL-261luc:IL-12 and GL-261luc:IL-23 cells; data representative of ≥3 independent experiments: (A) MHCI (H-2D(b)) and MHCII (I-A(b)) expression. (B) ^{3}[H]-Thymidine incorporation of GL-261 cells/well, error bars represent SD, one-way ANOVA with Bonferroni post-test; *, P < 0.05; **, P < 0.01; ***, P < 0.001. (C–E) GL-261 cells were injected into the right striatum of WT animals. (left) BLI emitted from a circular region of interest (ROI) around the tumor site, each trace represents BLI of an individual animal; (right) survival plot of the same experiment, two independent experiments pooled; Log-Rank test; *, P < 0.05; **, P < 0.01; ***, P < 0.001. (C) Survival of mice challenged with GL-261 or GL-261luc:Fc ($n ≥ 8$/group), with GL-261luc:Fc or GL-261luc:IL-23 cells (D; $n ≥ 10$/group, P = 0.0432) or GL-261luc:Fc or GL-261luc:IL-12 cells (E; $n = 12$/group, P = 0.0002). (F) Largest cross-section of representative tumors ($n = 6$/group) at day 35, brown: F4/80 immunoreactivity; counterstained with hematoxylin, arrow head: GL-261luc:IL-12 tumor. Bar, 2 mm.

of NK cells and the T_H1 hallmark cytokine IFN–γ compared with a study where IL–12 was produced in situ and mouse mutants were used (Vetter et al., 2009). Some of these studies have investigated tumors derived from s.c. injection of glioma cell lines (Joki et al., 1999). However, in s.c. tumors, a subpopulation of ILCs seems to be crucial for IL–12–mediated tumor control, regardless of the tissue origin of the tumor cells used (Eisenring et al., 2010). Using an IL–12–expressing syngeneic glioma cell line and various genetic mutants, we established T cells as the crucial effector cell type of IL–12–mediated glioma rejection. Further characterization of the tumor–infiltrating T cells revealed robust expression of cytotoxic T lymphocyte–associated antigen 4 (CTLA-4; Fig. 2 F).

CTLA-4 is the prototypic co-inhibitory receptor limiting T cell responses and its blockade has been shown to boost anti-tumor activity in metastatic melanoma in patients (Hodi et al., 2010; Walker and Sansom, 2011). We observed a slight increase in the numbers of CTLA-4–positive $CD4^+FoxP3^-$ T cells in GL-261luc:IL-12 tumors and an increase in the expression levels of CTLA-4 in T reg cells (Fig. 2 G).

Next, we explored the possibility of combining intratumoral (i.t.) IL–12 therapy with blockade of cytotoxic CTLA-4. For this, we expressed and purified IL-12Fc, which has biological activity that is identical to heterodimeric IL–12 (Fig. 3 A; Eisenring et al., 2010). Switching to a therapeutic setting, we challenged mice with GL-261luc:Fc, and then allowed for
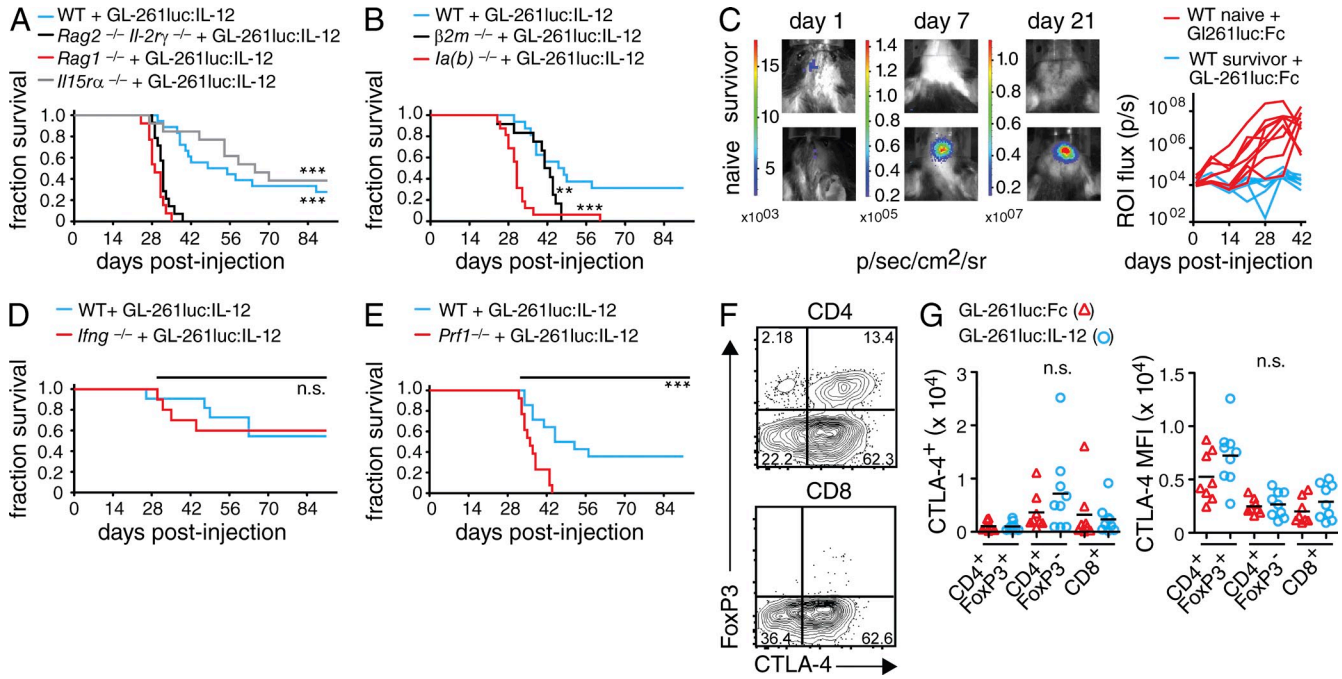
Figure 2. T cell dependency of IL–12–mediated glioma rejection. (A, B and D, E) GL-261luc:IL-12 cells were implanted i.c. into various immunodeficient mouse strains. Animals were monitored for up to 91 d; Log-Rank test; *, P < 0.05; **, P < 0.01; ***, P < 0.001. (A) Survival of WT, *Rag2−/− Il2rg−/−*, *Rag1−/−*, and *Il15ra−/−* mice (n ≥ 13/group); p(*Rag2−/− Il2rg−/−* vs. WT), p(*Rag1−/−* vs. WT), p(*Rag2−/− Il2rg−/−* vs. *Il15ra−/−*) and p(*Rag1−/−* vs. *Il15ra−/−*) < 0.0001. (B) Survival of WT, β*2m−/−* and *Ia(b)−/−* mice (n ≥ 12/group); p(β*2m−/−* vs. WT) = 0.0052, p(*Ia(b)−/−* vs. WT) < 0.0001. (C) Rechallenge of naive WT animals and survivors (that had been previously challenged with GL-261luc:IL-12 in the contralateral hemisphere) with GL-261luc:Fc cells; (left) representative BLI at days 1, 7, and 21; (right) BLI quantification (n ≥ 7/group). (D) Survival of WT and *Ifng−/−* mice (n ≥ 10/group) injected with GL-261luc:IL-12 (E) Survival of WT and *Prf1−/−* mice (n ≥ 13/group); p(*Prf1−/−* vs. WT) = 0.0005. (F and G) WT mice were implanted i.c. with GL-261luc:Fc or GL-261luc:IL-12 and analyzed for TILs at day 21 using flow cytometry. (F) Representative contour plot (GL-261luc:Fc TILs gated on live CD45^{hi}/CD11b^{-}/NK1.1^{-} cells). (G) Number (left) of CTLA-4 positive cells and CTLA-4 mean fluorescent intensity (MFI, right) for live CD4^{+}FoxP3^{+}, CD4+FoxP3^{-}, or CD8^{+} T cells (n ≥ 8/group). One-way ANOVA with Bonferroni post-test; pooled data from two to three independent experiments each; *, P < 0.05; **, P < 0.01; ***, P < 0.001.

tumor growth until day 21. At this time point, the cerebral tumor was clearly visible and comparable among the groups as quantified by BLI (Fig. 3, B and C). We implanted osmotic minipumps to deliver purified IL-12Fc over a 28-d period directly into the bulk tumor. Local IL-12Fc treatment was combined with systemic administration of antibodies against CTLA-4. Monotherapies with i.t. application of IL-12Fc or systemic anti–CTLA-4 alone conferred only a minor or no survival advantage, respectively (Fig. 3 B). Strikingly, local IL-12Fc administration directly into the tumor site in combination with systemic CTLA-4 blockade led to a full remission in most mice. We observed similar survival rates treating GL-261luc:Fc- or GL-261-derived tumors with this combination therapy (unpublished data), indicating its effectiveness independent of luciferase as xeno/neo antigen.

2 wk after the start of treatment (day 35 after injection), signs of a successful antitumor immune response were visible for IL-12Fc/PBS and IL-12Fc/αCTLA-4 treated animals in histological overviews (Fig. 3 C). Further analysis revealed a dramatic increase in CD4^{+} T cells upon IL-12Fc treatment, whereas CD8^{+} T cells increased, especially upon concomitant anti–CTLA-4 treatment (Fig. 3, D and E). In contrast to T cells, NK cells were present in high numbers in PBS/PBS- or

PBS/αCTLA-4–treated tumors, but decreased considerably upon IL-12Fc treatment (Fig. 3, D and E). This observation was confirmed by flow cytometry (Fig. 4 A). The drop in NK cells suggests that initially reacting NK cells may subsequently be replaced by T eff cells.

FACS quantification further revealed an increase in total CD4^{+} T cells between days 21 and 35 after injection (Fig. 4 A). Most importantly, there was a strong increase in the frequency of CD4^{+} T cells producing IFN-γ, but a profound reduction of FoxP3^{+} cells (Fig. 4 A). This was also reflected in the ratios of CD8^{+} per CD4^{+}FoxP3^{+} cells and especially CD4^{+}IFN-γ^{+} per CD4^{+}FoxP3^{+} cells, revealing a significant difference between IL-12Fc monotherapy and IL-12Fc/αCTLA-4 combination therapy (Fig. 4 B). The fact that accumulation of T reg cells is a key feature of human GB and correlates with outcome (Jacobs et al., 2010) underlines the clinical significance of the treatment approach used here. During and after treatment, we did not observe any overt symptoms of autoimmunity such as weight loss or paralysis (data not shown). Still, 91 d after tumor inoculation, histological assessment of the brain tissue of surviving animals did show residual infiltrates consisting mainly of CD4^{+} T cells and NK cells (Fig. 3, C and D).
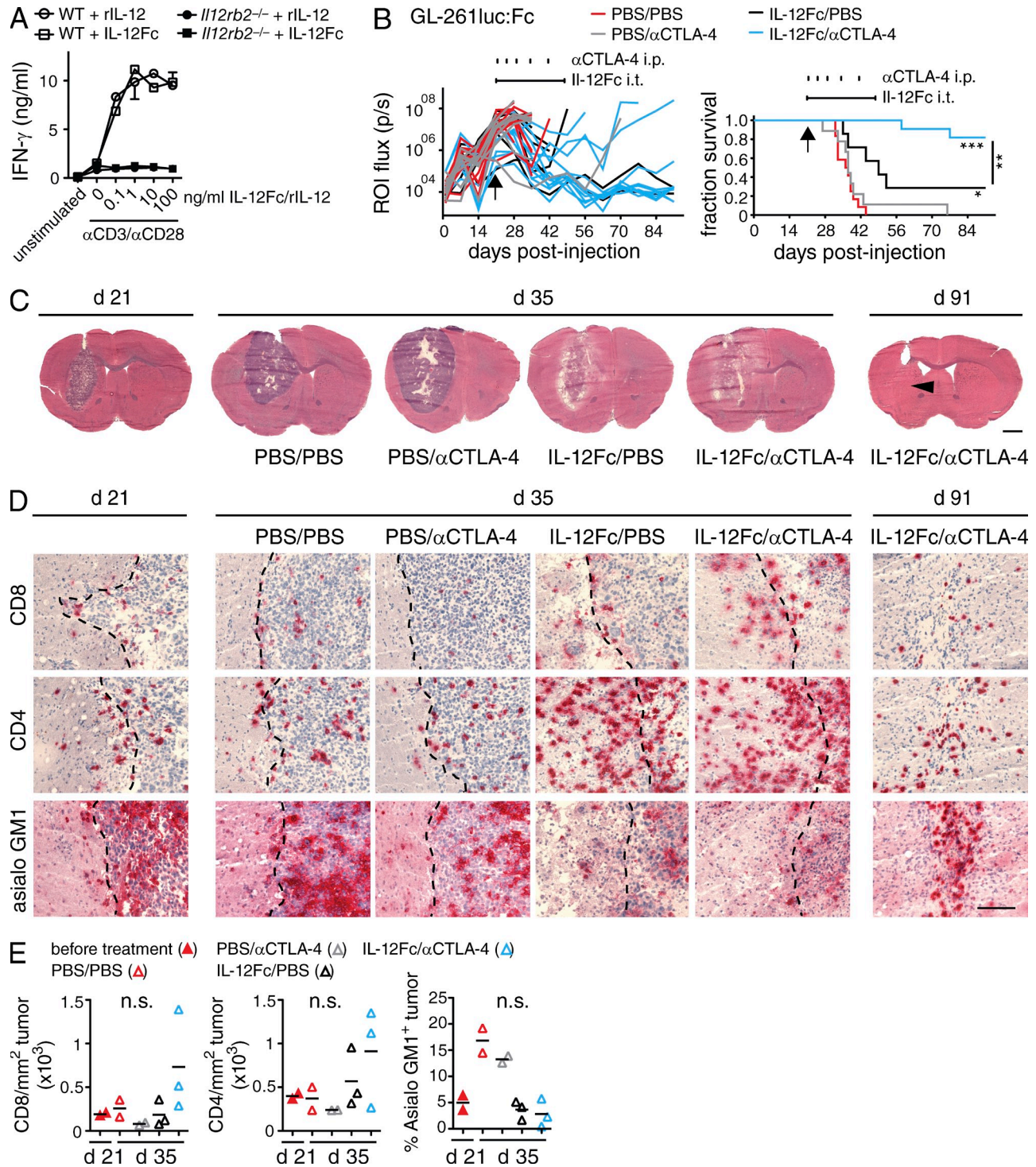
Figure 3. Local administration of IL–12Fc in established GB in combination with systemic CTLA–4 blockade induces tumor clearance. (A) IFN-γ production of WT or *Il12rb2*$^{-/-}$ splenocytes stimulated with anti-CD3 and anti-CD28 mAbs and increasing amounts of heterodimeric IL-12 (rIL-12) or IL-12Fc; one out of three experiments shown. (B) WT mice were injected i.c. with GL-261luc:Fc cells. On day 21 after injection, osmotic minipumps delivering IL-12Fc or PBS intratumorally (i.t.) were implanted as indicated by a horizontal line above graphs. In addition, animals received i.p. injections with αCTLA-4 mAbs or PBS, indicated by vertical tick marks; *n* = 7–12/group; three independent experiments pooled. Log-rank test; *, P < 0.05; **, P < 0.01; ***, P < 0.001; p(IL-12Fc/PBS vs. IL-12Fc/αCTLA-4) = 0.0061, p(PBS/PBS vs. IL-12Fc/PBS) = 0.0160, p(PBS/PBS vs. IL-12Fc/αCTLA-4), and p(PBS/αCTLA-4 vs. IL-12Fc/αCTLA-4) < 0.0001. (C–E) Histological analysis of GL-261luc:Fc tumors at day 21, 2 wk after initiation of treatment (day 35) and at the end of the experiment (day 91). (C) Overviews, arrowhead indicates former tumor center. Bar, 2 mm. (D) Higher magnification, sections show CD4, CD8, and asialo GM1 immunoreactivity (red); tumor margin is indicated (dotted line. Bar, 200 µm. (E) Quantification of TILs/tumor area on histological sections, each dot represents mean of a single animal; one-way ANOVA with Bonferroni post-test; one of two independent experiments shown; *, P < 0.05; **, P < 0.01; ***, P < 0.001.
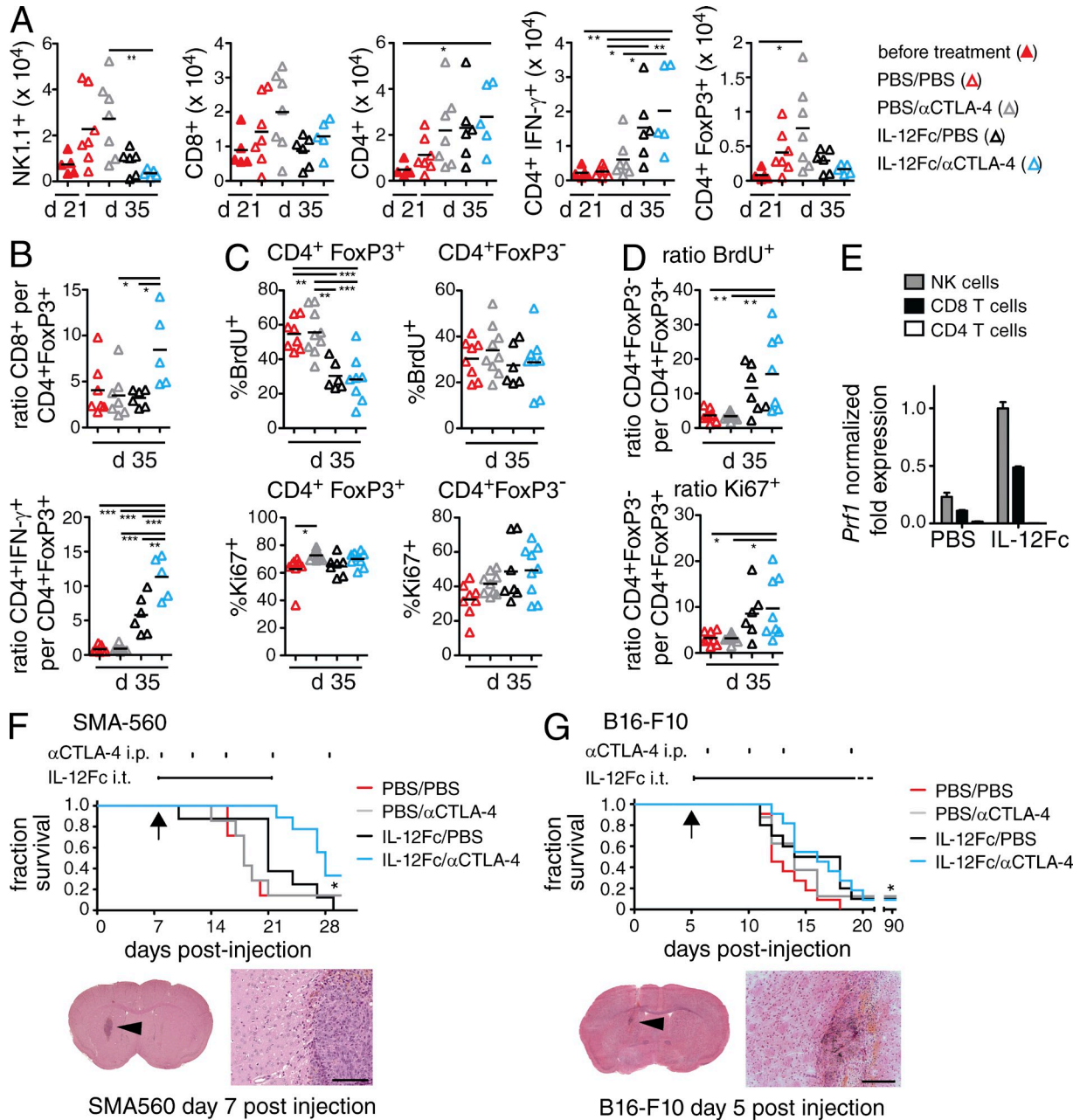
Figure 4. Combination treatment leads to a shift from T reg to T eff cells within the tumor. (A–D) TILs of tumor-bearing brains were analyzed by flow cytometry at days 21 and 35, 2 wk after initiation of treatment; two independent experiments pooled, one-way ANOVA with Bonferroni post-test; *, $P < 0.05$; **, $P < 0.01$; ***, $P < 0.001$. (A) Total number of NK and T cells, pregated on CD45^{hi}/CD11b$^-$ cells. (B) Ratio of CD8$^+$ and CD4$^+$IFN-γ^+ T cells per CD4$^+$FoxP3$^+$ T cells; $n \geq 5$/group; (C) BrdU and Ki67 labeling of T reg and T eff cells (pregated on CD45$^+$CD11b$^-$NK1.1$^-$) in percent positive cells and (D) ratio of total numbers of T reg versus T eff cells; $n \geq 6$/group; (E) *Perforin-1* gene expression in TILs sorted from treated animals ($n = 3$/group). Shown is the normalized fold expression (ΔCT) in relation to HPRT expression; error bars are the SEM of replicate wells. Individual samples were pooled before sorting, which precluded statistical assessment. VM/Dk or B6 WT mice were injected i.c. with SMA-560 cells ($n \geq 7$/group; F) and B16-F10 melanoma cells ($n \geq 10$/group; G), respectively. Arrows show initiation of treatment. Osmotic minipumps delivered IL-12Fc or PBS i.t. as indicated by a horizontal line above graph. In addition, animals received i.p. injections with αCTLA-4 mAbs or PBS, indicated by vertical tick marks; two independent experiments pooled. Survival statistics according to Log-rank test; *, $P < 0.05$; **, $P < 0.01$; ***, $P < 0.001$. (F) p(PBS/PBS vs. IL-12Fc/αCTLA-4) = 0.0182, p(IL-12Fc/PBS vs. IL-12Fc/αCTLA-4) = 0.0155, p(PBS/αCTLA-4 vs. IL-12Fc/αCTLA-4) = 0.0177. (G) p(PBS/PBS vs. IL-12Fc/αCTLA-4) = 0.0174. Histology below survival curves shows tumor burden at initiation of treatment, overview pictures. and higher magnification pictures of the indicated regions (arrowheads). Bars: 100 µm (F); 200 µm (G).

To understand the mechanism by which IL-12Fc/αCTLA-4 combination therapy alters the composition of TILs, most notably the drop in T reg cells and increase in T eff cells, we analyzed proliferation of TILs upon treatment. By assessing BrdU incorporation and Ki67 labeling, we found that IL-12Fc, as well as IL-12Fc/αCTLA-4 combination therapy led to a selective drop of BrdU$^+$ T reg cells during the second week of treatment. At day 35, the T eff cell population did however display a higher percentage of Ki67–positive cells (Fig. 4 C), resulting in a significant increase in the ratio of FoxP3$^-$ versus FoxP3$^+$ CD4 T cells regarding BrdU incorporation and Ki67 labeling (Fig. 4 D). We did not observe significant differences in Annexin V labeling, a marker for apoptosis, most likely due to the fact that apoptotic cells are rapidly cleared by phagocytes in vivo (unpublished data). The mechanism by which CTLA-4 blockade inhibits T reg cell function remains a subject of intense debate (Walker and Sansom, 2011). Recent studies demonstrate that selective opsonization of T reg cells with CTLA-4 antibodies can elicit potent antibody-dependent cell-mediated cytotoxicity (ADCC) within the tumor site (Selby et al., 2013; Simpson et al., 2013). In regard to the tumor-suppressing effector cells, IL-12 increased the expression of perforin-1 in CD8 T cells and NK cells, but not in CD4 cells (Fig. 4 E), indicating that CTLs are ultimately responsible for tumor control.

We next tested the treatment regimen in a different model of GB. SMA-560 is derived from a spontaneous murine astrocytoma (Uhl et al., 2004). Here, we initiated treatment on day 7 after tumor cell implantation. Also, in this genetically different mouse strain (VM/Dk), we found the combination therapy to confer a significant survival advantage (Fig. 4 F).

The poor activity of CTLA-4 monotherapy observed in our study contrasts with previous studies using similar models (Fecci et al., 2007; Grauer et al., 2007; Agarwalla et al., 2012). In those studies CTLA-4 blockade was initiated at much earlier time points after seeding, the disease course progressed at a slower pace, and/or a different mAb was used in treatments. We used a different anti–CTLA-4 mAb (9D9, IgG2b), which has been reported to confer weaker ADCC of T reg cells than the 9H10 hamster mAb used by Fecci et al. (2007; Selby et al., 2013; Simpson et al., 2013). It is therefore tempting to speculate that the combination of i.t. IL-12Fc in combination with systemic CTLA-4 blockade through a strong ADCC-inducing mAb may yield even better synergy. To expand our treatment strategy toward other types of cancers, we explored intracranial implantation of B16:F10 melanoma cells. B16 is an extremely aggressive melanoma cell line and poorly immunogenic (Becker et al., 2010). In this rapidly progressing model of intracranial melanoma, only combination therapy led to a significant, albeit very modest survival advantage when compared with vehicle controls (Fig. 4 G).

Systemic anti–CTLA-4 treatment is FDA-approved for metastatic melanoma based on clinical trials demonstrating clinical benefit (Hodi et al., 2010) and has been further tested for various other solid cancers (Grosso and Jure-Kunkel, 2013). In light of the data presented here, a combination therapy consisting of systemic checkpoint blockade and local administration of IL-12 is a highly promising candidate for swift clinical translation in GB.

MATERIALS AND METHODS

Animals. C57BL/6 mice were obtained from Janvier; $b2m^{-/-}$, $Ia(b)^{-/-}$, $Il12rb2^{-/-}$, $Rag1^{-/-}$, $Rag2^{-/-} Il2rg^{-/-}$, $Prf1^{-/-}$, and $Ifng^{-/-}$ mice were obtained from The Jackson Laboratory. $Il15ra^{-/-}$ mice were provided by S. Bulfone-Paus (Forschungszentrum Borstel, Borstel, Germany) and VM/Dk mice are bred in our laboratory. All animals were kept in house according to institutional guidelines under specific pathogen–free conditions at a 12-h light/dark cycle with food and water provided ad libitum. All animal experiments were performed according to institutional guidelines and approved by the Swiss cantonary veterinary office (licenses 16/2009; 65/2012).

Murine tumor cell lines. GL-261 cells (provided by A. Fontana, Experimental Immunology, University of Zurich, Zurich, Switzerland), which are syngeneic in C57BL/6 mice, were stably transfected with pGl3-ctrl and pGK-Puro (Promega) and selected with puromycin (Sigma-Aldrich) to generate luciferase-stable GL-261 cells. A single clone was isolated by limiting dilution and passaged in vivo by intracranial tumor inoculation. Subsequently, cells were transfected with pCEP4-mIgG3, pCEP4-mIl-12mIgG3, or pCEP4-mIl-23mIgG3, and cytokine production was detected by ELISA and RT-PCR, as previously described (Eisenring et al., 2010). SMA-560 spontaneous murine astrocytoma cells were characterized previously (Uhl et al., 2004). B16-F10 C57BL/6 murine melanoma cells were purchased from American Type Culture Collection.

Proliferation assay. 5,000 cells/well were plated into a 96-well plate in triplicates. Medium containing 0.5 mCi/ml of [^{3}H]thymidine was added, and 4 d later the incorporation was assessed using a Filtermate Collector (Applied Biosystems) and a scintillation counter (MicroBeta Trilux 1450; Wallac).

Expression and purification of IL-12Fc. IL-12Fc was expressed in 293T cells. The protein was purified from supernatant over a protein G column (1 ml; HiTrap; GE Healthcare) and eluted with 0.1 M glycine, pH 2.0, using a purifier (ÄktaPrime) and dialyzed overnight in PBS, pH 7.4. Concentration and purity of IL-12Fc were measured by ELISA (OptEIA mouse IL-12/23p40; BD) and SDS-PAGE (silver staining and immunoblotting). IL-12Fc was detected with a rat anti–mouse IL-12p40 antibody (C17.8; BioExpress) and a goat anti–rat HRP coupled antibody (Jackson ImmunoResearch Laboratories).

Functional characterization of IL-12Fc. Splenocytes isolated from WT or $Il12rb2^{-/-}$ animals were plated in duplicates at a density of 10^5 cells/well in RPMI medium (GIBCO BRL Invitrogen) supplemented with 10% fetal calf serum in 96-well plates and stimulated with either recombinant murine IL-12 (PeproTech) or IL-12Fc. Splenocytes were cultured in the presence of 0.5 µg/ml of anti-mouse CD3 (2C11, BioExpress) and anti-CD28 antibodies (37N, BioExpress). After two days of culture supernatant was harvested and IFN-γ detected with an anti-mouse IFN-γ ELISA kit (OptEIA mouse IFN-γ BD).

Orthotopic glioma inoculation. In brief, 6–10-wk-old mice were i.p. injected with fluniximin (Biokema; 5 mg/kg body weight) before being anesthetized with 3–5% Isoflurane (Minrad) in an induction chamber. Anesthesia on the stereotactic frame (David Kopf Instruments) was maintained at 3% Isoflurane delivered through a nose adaptor, A blunt-ended syringe (Hamilton; 75N, 26s/2"/2, 5 µl) was placed 1.5 mm lateral and 1 mm frontal of bregma. The needle was lowered into the burr hole to a depth of 4 mm below the dura surface and retracted 1 mm to form a small reservoir. Using a microinjection pump (UMP-3; World precision Instruments Inc.), 2×10^4 GL-261 (500 SMA-560 or 50 B16-F10) cells were injected in a volume of 2 µl at 1 µl/min. After leaving the needle in place for 2 min, it was retracted at 1 mm/min. The burr hole was closed with bone wax (Aesculap; Braun) and the scalp wound was sealed with tissue glue (Indermil; Henkel).

In vivo bioluminescent imaging. Tumor-bearing mice were injected with D-Luciferin (150 mg/kg body weight; Caliper Life Sciences). Animals were transferred to the dark chamber of a Xenogen IVIS 100 (Caliper Life Sciences) imaging system and luminescence was recorded. Data were subsequently analyzed using Living Image 2.5 software (Caliper Life Sciences). A circular region of interest (ROI; 1.46 cm diam) was defined around the tumor site and photon flux of this region was read out and plotted.

Treatment of established gliomas. At d 21 after implantation of the GL-261luc:Fc glioma cells, the tumor-bearing animals were evenly distributed among experimental groups based on their ROI-photon flux. Animals with an ROI flux of less than 10^5 p/s were considered as non- or slow-takers and excluded. Osmotic pumps (model 2004, 0.25 µl/h; Alzet) were filled with murine IL-12Fc (8.33 ng/µl in PBS, 50 ng/24 h) or PBS alone and primed at 37°C in PBS. Implantation of osmotic minipumps has been described previously (vom Berg et al., 2012). The previous burr hole of the glioma injection was located, the bone wax and periosteal bone was removed, and the infusion cannula was lowered through the burr hole 3 mm into the putative center of the tumor. Pumps were explanted at day 49. Five doses of anti–mouse-CTLA-4 mouse-IgG2b antibodies (clone 9D9; BioExpress) or an equivalent volume of PBS were i.p. injected at days 1 (200 µg), 5 (100 µg), 8 (100 µg), 14 (100 µg), and 21 (100 µg) after pump implantation. For treatment of established B16-F10–derived brain tumors, pumps were implanted at day 5 after injection, for treatment of established SMA-560 tumors, pumps (model 1004, 0.25 µl/h; Alzet, filled with 41.65 ng/µl IL-12Fc in PBS; 250 ng/24 h) were implanted at day 7 after injection and explanted at day 21. Anti–mouse-CTLA-4 mouse-IgG2b antibodies (clone 9D9; BioExpress) were administered according to the aforementioned dosing scheme.

Survival analysis. Tumor-bearing animals were monitored by BLI, checked for neurological symptoms and weighed weekly until day 21 after glioma inoculation. From day 21 onwards animals were checked daily. Animals that showed symptoms such as apathy, severe hunchback posture, or weight loss exceeding 20% were euthanized. SMA-560 or B16-F10 tumor-bearing mice were scored daily starting at day 14 (or day 5, respectively) until the end of the experiment according to the same scheme.

Flow cytometry. The following antibodies were used for flow cytometric analyses: anti-CD45 (30-F11; BioLegend), anti-CD11b (M1/70; BD), anti-CD4 (Gk1.5; BioLegend or BD), anti-CD8 (53–6.7; BioLegend or BD), anti-CD3 (17A2; BioLegend), anti-H-2D(b) (24–14-8; eBioscience), anti–I-A(b) (AF6-120.1; BD), anti-NK1.1 (PK136; BD), anti-FoxP3 (FJK-16s; eBioscience), anti-BrdU (Bu20a; eBioscience), anti-Ki67 (SOLA15; eBioscience), Annexin V (eBioscience), anti-CTLA-4 (UC10-F10; BD), and anti–IFN-γ (XMG1.2; BD). For the exclusion of dead cells, we used the Zombie Aqua fixable viability kit (BioLegend). Doublets were excluded based on FSC-A/FSC-H. The frontal part of the tumor-bearing cerebral hemisphere was harvested, and cells were prepared for flow cytometry as described previously (vom Berg et al., 2012). Cells were restimulated for 3 h at 37°C and 5% CO_2 in RPMI 1640 medium. RPMI 1640 was supplemented with 10% FCS and phorbol 12-myristate 13-acetate (50 ng/ml), ionomycin (500 ng/µl), and brefeldin A (1 µl/ml medium; GolgiPlug; BD). For in vivo proliferation analysis, BrdU (Sigma-Aldrich) was added to drinking water (80 mg/100 ml) and changed every second day during the second week of treatment (day 28–35). For analysis of proliferation or apoptosis, cells were not restimulated. Intracellular cytokine, transcription factor, CTLA-4, BrdU, and Ki67 staining was performed using the eBioscience FoxP3 staining buffer set following the manufacturer's instructions. Acquisition was performed on a LSRII Fortessa flow cytometer (BD), sorting was performed on a FACSAria II. Data analysis was performed using FlowJo Version 9.6.4 (Tree Star).

Complementary DNA synthesis and quantitative real-time PCR. Respective populations were FACS sorted, gating on NK cells (live singlets, CD45^{hi}NK1.1^{+}CD3^{−}), CD4 T cells (live singlets, CD45^{hi}NK1.1^{−}CD3^{+}CD11b^{−}CD4^{+}), and CD8 T cells (live singlets, CD45^{hi}NK1.1^{−}CD3^{+}CD11b^{−}CD8^{+}).

Cells were frozen immediately, lysed and RNA isolated. Poly-d(T) primers were used for synthesis of complementary DNA. TaqMan probes and primers for hypoxanthine-guanine phosphoribosyltransferase (HPRT) and Perforin (*prf1*) were used for quantitative real-time PCR using a CFX384 Cycler (Bio-Rad Laboratories). Subsequent analyses were performed with Bio-Rad CFX Manager software using the ΔCt method. The specificity of amplification was also assessed by gel electrophoresis.

Histology. For histology, animals were euthanized with CO_2, transcardially perfused with ice-cold PBS, and decapitated. The brain was removed and the frontal part of the cerebrum was embedded in optimal cutting temperature compound (O.C.T.; Sakura) and snap-frozen in liquid nitrogen. Immunostaining of cryosections was performed as described previously (Eisenring et al., 2010). Alternatively, sections were stained with hematoxylin and eosin. Brains were also fixed in 4% formalin, embedded in paraffin and 2–3 µm sections were processed. Pictures were generated using an Olympus BX41 light microscope equipped with an Olympus ColorView IIIu camera and Olympus cell B image acquisition software. Whole slides were also scanned with a Zeiss Mirax Midi slidescanner, equipped with a 20× objective (NA 0.8) and 3CCD color camera (1360 × 1024 pixel, size 0.23 µm) and analyzed using Panoramic viewer 1.14.50 RTM and the HistoQuant plugin (both 3DHISTECH). Tumor boundaries were manually outlined and either area covered by staining and/or number of objects stained where quantified using the batch processing function. Images shown in figures were processed with Adobe Photoshop CS5.

Statistical analysis. For all nonsurvival analyses of two experimental groups, an unpaired, two-tailed Student's *t* test was performed. For all nonsurvival analyses of three or more experimental groups, a one-way ANOVA with Bonferroni posttest was performed. For statistical analysis of Kaplan-Meier survival curves, a Log-rank (Mantel-Cox) test was used to calculate the p-values indicated in respective experiments. P-values <0.05 were considered statistically significant and indicated in figures as asterisks (*, P < 0.05; **, P < 0.01; ***, P < 0.001). All quantitative analysis was performed with GraphPad Prism version 5.0a for Mac OSX (GraphPad Software, Inc).

REFERENCES

Agarwalla, P., Z. Barnard, P. Fecci, G. Dranoff, and W.T. Curry Jr. 2012. Sequential immunotherapy by vaccination with GM-CSF-expressing glioma cells and CTLA-4 blockade effectively treats established murine intracranial tumors. *J. Immunother.* 35:385–389. http://dx.doi.org/10.1097/CJI.0b013e3182562d59

Atkins, M.B., M.J. Robertson, M. Gordon, M.T. Lotze, M. DeCoste, J.S. DuBois, J. Ritz, A.B. Sandler, H.D. Edington, P.D. Garzone, et al. 1997.

Phase I evaluation of intravenous recombinant human interleukin 12 in patients with advanced malignancies. *Clin. Cancer Res.* 3:409–417.

Becker, J.C., R. Houben, D. Schrama, H. Voigt, S. Ugurel, and R.A. Reisfeld. 2010. Mouse models for melanoma: a personal perspective. *Exp. Dermatol.* 19:157–164. http://dx.doi.org/10.1111/j.1600-0625.2009.00986.x

Colombo, M.P., and G. Trinchieri. 2002. Interleukin-12 in anti-tumor immunity and immunotherapy. *Cytokine Growth Factor Rev.* 13:155–168. http://dx.doi.org/10.1016/S1359-6101(01)00032-6

Cui, J., T. Shin, T. Kawano, H. Sato, E. Kondo, I. Toura, Y. Kaneko, H. Koseki, M. Kanno, and M. Taniguchi. 1997. Requirement for Valpha14 NKT cells in IL-12-mediated rejection of tumors. *Science.* 278:1623–1626. http://dx.doi.org/10.1126/science.278.5343.1623

Daga, A., A.M. Orengo, R.M. Gangemi, D. Marubbi, M. Perera, A. Comes, S. Ferrini, and G. Corte. 2007. Glioma immunotherapy by IL-21 gene-modified cells or by recombinant IL-21 involves antibody responses. *Int. J. Cancer.* 121:1756–1763. http://dx.doi.org/10.1002/ijc.22901

Eisenring, M., J. vom Berg, G. Kristiansen, E. Saller, and B. Becher. 2010. IL-12 initiates tumor rejection via lymphoid tissue-inducer cells bearing the natural cytotoxicity receptor NKp46. *Nat. Immunol.* 11:1030–1038. http://dx.doi.org/10.1038/ni.1947

Fecci, P.E., H. Ochiai, D.A. Mitchell, P.M. Grossi, A.E. Sweeney, G.E. Archer, T. Cummings, J.P. Allison, D.D. Bigner, and J.H. Sampson. 2007. Systemic CTLA-4 blockade ameliorates glioma-induced changes to the CD4+ T cell compartment without affecting regulatory T-cell function. *Clin. Cancer Res.* 13:2158–2167. http://dx.doi.org/10.1158/1078-0432.CCR-06-2070

Gordy, L.E., J.S. Bezbradica, A.I. Flyak, C.T. Spencer, A. Dunkle, J. Sun, A.K. Stanic, M.R. Boothby, Y.W. He, Z. Zhao, et al. 2011. IL-15 regulates homeostasis and terminal maturation of NKT cells. *J. Immunol.* 187:6335–6345. http://dx.doi.org/10.4049/jimmunol.1003965

Grauer, O.M., S. Nierkens, E. Bennink, L.W. Toonen, L. Boon, P. Wesseling, R.P. Sutmuller, and G.J. Adema. 2007. CD4+FoxP3+ regulatory T cells gradually accumulate in gliomas during tumor growth and efficiently suppress antiglioma immune responses in vivo. *Int. J. Cancer.* 121:95–105. http://dx.doi.org/10.1002/ijc.22607

Grosso, J.F., and M.N. Jure-Kunkel. 2013. CTLA-4 blockade in tumor models: an overview of preclinical and translational research. *Cancer Immun.* 13:5.

Hodi, F.S., S.J. O'Day, D.F. McDermott, R.W. Weber, J.A. Sosman, J.B. Haanen, R. Gonzalez, C. Robert, D. Schadendorf, J.C. Hassel, et al. 2010. Improved survival with ipilimumab in patients with metastatic melanoma. *N. Engl. J. Med.* 363:711–723. http://dx.doi.org/10.1056/NEJMoa1003466

Hu, J., X. Yuan, M.L. Belladonna, J.M. Ong, S. Wachsmann-Hogiu, D.L. Farkas, K.L. Black, and J.S. Yu. 2006. Induction of potent antitumor immunity by intratumoral injection of interleukin 23-transduced dendritic cells. *Cancer Res.* 66:8887–8896. http://dx.doi.org/10.1158/0008-5472.CAN-05-3448

Jacobs, J.F., A.J. Idema, K.F. Bol, J.A. Grotenhuis, I.J. de Vries, P. Wesseling, and G.J. Adema. 2010. Prognostic significance and mechanism of Treg infiltration in human brain tumors. *J. Neuroimmunol.* 225:195–199. http://dx.doi.org/10.1016/j.jneuroim.2010.05.020

Joki, T., T. Kikuchi, Y. Akasaki, S. Saitoh, T. Abe, and T. Ohno. 1999. Induction of effective antitumor immunity in a mouse brain tumor model using B7-1 (CD80) and intercellular adhesive molecule 1 (ICAM-1; CD54) transfection and recombinant interleukin 12. *Int. J. Cancer.* 82:714–720. http://dx.doi.org/10.1002/(SICI)1097-0215(19990827)82:5<714::AID-IJC15>3.0.CO;2-Q

Kodama, T., K. Takeda, O. Shimozato, Y. Hayakawa, M. Atsuta, K. Kobayashi, M. Ito, H. Yagita, and K. Okumura. 1999. Perforin-dependent NK cell cytotoxicity is sufficient for anti-metastatic effect of IL-12. *Eur. J. Immunol.* 29:1390–1396. http://dx.doi.org/10.1002/(SICI)1521-4141(199904)29:04<1390::AID-IMMU1390>3.0.CO;2-C

Langowski, J.L., X. Zhang, L. Wu, J.D. Mattson, T. Chen, K. Smith, B. Basham, T. McClanahan, R.A. Kastelein, and M. Oft. 2006. IL-23 promotes tumour incidence and growth. *Nature.* 442:461–465. http://dx.doi.org/10.1038/nature04808

Leonard, J.P., M.L. Sherman, G.L. Fisher, L.J. Buchanan, G. Larsen, M.B. Atkins, J.A. Sosman, J.P. Dutcher, N.J. Vogelzang, and J.L. Ryan. 1997.

Effects of single-dose interleukin-12 exposure on interleukin-12-associated toxicity and interferon-gamma production. *Blood.* 90:2541–2548.

Liu, Y., M. Ehtesham, K. Samoto, C.J. Wheeler, R.C. Thompson, L.P. Villarreal, K.L. Black, and J.S. Yu. 2002. In situ adenoviral interleukin 12 gene transfer confers potent and long-lasting cytotoxic immunity in glioma. *Cancer Gene Ther.* 9:9–15. http://dx.doi.org/10.1038/sj.cgt.7700399

Lo, C.H., S.C. Lee, P.Y. Wu, W.Y. Pan, J. Su, C.W. Cheng, S.R. Roffler, B.L. Chiang, C.N. Lee, C.W. Wu, and M.H. Tao. 2003. Antitumor and antimetastatic activity of IL-23. *J. Immunol.* 171:600–607.

Ngiow, S.F., M.W. Teng, and M.J. Smyth. 2013. A balance of interleukin-12 and –23 in cancer. *Trends Immunol.* 34:548–555. http://dx.doi.org/10.1016/j.it.2013.07.004

Selby, M.J., J.J. Engelhardt, M. Quigley, K.A. Henning, T. Chen, M. Srinivasan, and A.J. Korman. 2013. Anti-CTLA-4 Antibodies of IgG2a Isotype Enhance Antitumor Activity through Reduction of Intratumoral Regulatory T Cells. *Cancer Immunol. Res.* doi: 10.1158/2326-6066.CIR-13-0013.

Simpson, T.R., F. Li, W. Montalvo-Ortiz, M.A. Sepulveda, K. Bergerhoff, F. Arce, C. Roddie, J.Y. Henry, H. Yagita, J.D. Wolchok, et al. 2013. Fc-dependent depletion of tumor-infiltrating regulatory T cells co-defines the efficacy of anti-CTLA-4 therapy against melanoma. *J. Exp. Med.* 210:1695–1710. http://dx.doi.org/10.1084/jem.20130579

Szatmári, T., K. Lumniczky, S. Désaknai, S. Trajcevski, E.J. Hídvégi, H. Hamada, and G. Sáfrány. 2006. Detailed characterization of the mouse glioma 261 tumor model for experimental glioblastoma therapy. *Cancer Sci.* 97:546–553. http://dx.doi.org/10.1111/j.1349-7006.2006.00208.x

Uhl, M., S. Aulwurm, J. Wischhusen, M. Weiler, J.Y. Ma, R. Almirez, R. Mangadu, Y.W. Liu, M. Platten, U. Herrlinger, et al. 2004. SD-208, a novel transforming growth factor beta receptor I kinase inhibitor, inhibits growth and invasiveness and enhances immunogenicity of murine and human glioma cells in vitro and in vivo. *Cancer Res.* 64:7954–7961. http://dx.doi.org/10.1158/0008-5472.CAN-04-1013

Vetter, M., M.J. Hofer, E. Roth, H.P. Pircher, and A. Pagenstecher. 2009. Intracerebral interleukin 12 induces glioma rejection in the brain predominantly by CD8+ T cells and independently of interferon-gamma. *J. Neuropathol. Exp. Neurol.* 68:525–534. http://dx.doi.org/10.1097/NEN.0b013e3181a2afa0

Vom Berg, J., S. Prokop, K.R. Miller, J. Obst, R.E. Kälin, I. Lopategui-Cabezas, A. Wegner, F. Mair, C.G. Schipke, O. Peters, et al. 2012. Inhibition of IL-12/IL-23 signaling reduces Alzheimer's disease-like pathology and cognitive decline. *Nat. Med.* 18:1812–1819. http://dx.doi.org/10.1038/nm.2965

Walker, L.S., and D.M. Sansom. 2011. The emerging role of CTLA4 as a cell-extrinsic regulator of T cell responses. *Nat. Rev. Immunol.* 11:852–863. http://dx.doi.org/10.1038/nri3108

Weller, M., T. Cloughesy, J.R. Perry, and W. Wick. 2013. Standards of care for treatment of recurrent glioblastoma—are we there yet? *Neuro-oncol.* 15:4–27. http://dx.doi.org/10.1093/neuonc/nos273

Yamanaka, R., S.A. Zullo, J. Ramsey, N. Yajima, N. Tsuchiya, R. Tanaka, M. Blaese, and K.G. Xanthopoulos. 2002. Marked enhancement of antitumor immune responses in mouse brain tumor models by genetically modified dendritic cells producing Semliki Forest virus–mediated interleukin-12. *J. Neurosurg.* 97:611–618. http://dx.doi.org/10.3171/jns.2002.97.3.0611

Yamanaka, R., N. Tsuchiya, N. Yajima, J. Honma, H. Hasegawa, R. Tanaka, J. Ramsey, R.M. Blaese, and K.G. Xanthopoulos. 2003. Induction of an antitumor immunological response by an intratumoral injection of dendritic cells pulsed with genetically engineered Semliki Forest virus to produce interleukin-18 combined with the systemic administration of interleukin-12. *J. Neurosurg.* 99:746–753. http://dx.doi.org/10.3171/jns.2003.99.4.0746

Yuan, X., J. Hu, M.L. Belladonna, K.L. Black, and J.S. Yu. 2006. Interleukin-23-expressing bone marrow-derived neural stem-like cells exhibit antitumor activity against intracranial glioma. *Cancer Res.* 66:2630–2638. http://dx.doi.org/10.1158/0008-5472.CAN-05-1682